A field-pilot for passive bioremediation of As-rich acid mine drainage

L. Fernandez-Rojo, C. Casiot, E. Laroche, V. Tardy, O. Bruneel, S. Delpoux, A. Desoeuvre, G. Grapin, J. Savignac, J. Boisson, et al.

HAL Id: hal-02075868
https://hal.science/hal-02075868

A field-pilot for passive bioremediation of As-rich acid mine drainage

Fernandez-Rojo L.[a,1], Casiot C.[a*], Laroche E.[a,b], Tardy V.[a,2], Bruneel O.[a], Delpoux S.[a], Desoeuvre A.[a], Grapin G.[c], Savignac J.[c], Boisson J.[d], Morin G.[e], Battaglia-Brunet F.[b], Joulian C.[b], Héry M.[a]

[a] *HydroSciences Montpellier, Univ. Montpellier, CNRS, IRD, 163 rue Auguste Broussonnet, 34090 Montpellier, France*

[b] *French Geological Survey (BRGM), Geomicrobiology and environmental monitoring unit, 3, avenue Claude Guillemin, BP 36009, 45060 Orléans Cedex 2, France*

[c] *IRH Ingénieur Conseil, Anteagroup, 427 rue Lavoisier - CS 50155, 54714, Ludres Cedex, France*

[d] *IRH Ingénieur Conseil, Anteagroup, 197 avenue de Fronton, 31200, Toulouse, France*

[e] *Institut de Minéralogie, de Physique des Matériaux et de Cosmochimie (IMPMC), UMR 7590 CNRS-UPMC-IRD-MNHN, Sorbonne Universités, 4 place Jussieu, 75252 Paris cedex 05, France*

*Author for correspondence: Corinne Casiot

Tel +33 (0)4 67 14 33 56
Email: casiot@msem.univ-montp2.fr
Postal address: Université de Montpellier, Hydrosciences - CC57, 163 rue Auguste Broussonnet, 34090 Montpellier, France

Declarations of interest: none

---

[1] Present address: Institute of Environmental Assessment and Water Research (IDAEA), CSIC, Jordi Girona 18, 08034 Barcelona, Spain

[2] Present address: Irstea UR Milieux Aquatiques, Ecologie et Pollutions (UR MALY) – Irstea – 5 rue de la Doua BP 32108 F-69616 Villeurbanne Cedex, France

1 **Abstract**

2 A field-pilot bioreactor exploiting microbial iron (Fe) oxidation and subsequent arsenic

3 (As) and Fe co-precipitation was monitored during 6 months for the passive treatment

4 of As-rich acid mine drainage (AMD). It was implemented at the Carnoulès mining site

5 (southern France) where AMD contained 790–1315 mg L^{-1} Fe(II) and 84–152 mg L^{-1}

6 As, mainly as As(III) (78 − 83 %). The bioreactor consisted in five shallow trays of 1.5

7 m^2 in series, continuously fed with AMD by natural flow. We monitored the flow rate

8 and the water physico-chemistry including redox Fe and As speciation. Hydraulic

9 retention time (HRT) was calculated and the precipitates formed inside the bioreactor

10 were characterized (mineralogy, Fe and As content, As redox state). Since As(III)

11 oxidation improves As retention onto Fe minerals, bacteria with the capacity to oxidize

12 As(III) were quantified through their marker gene *aioA*. Arsenic removal yields in the

13 pilot ranged between 3 % to 97 % (average rate $(1.8 \pm 0.8) \times 10^{-8}$ mol L^{-1} s^{-1}), and were

14 positively correlated to HRT and inlet water dissolved oxygen concentration. Fe

15 removal yields did not exceed 11 % (average rate $(7 \pm 5) \times 10^{-8}$ mol L^{-1} s^{-1}). In the first

16 32 days, the precipitate contained tooeleite, a rare arsenite ferric sulfate mineral. Then,

17 it evolved toward an amorphous ferric arsenate phase. The As/Fe molar ratio and As(V)

18 to total As proportion increased from 0.29 to 0.86 and from ~20 % to 99 %,

19 respectively. The number of bacterial *aioA* gene copies increased ten-fold during the

20 first 48 days and stabilized thereafter. These results and the monitoring of arsenic

21 speciation in the inlet and the outlet water, provide evidences that As(III) oxidized in

22 the pilot. The biotreatment system we designed proved to be suitable for high As DMA.

23 The formation of sludge highly enriched into As(V) rather than As(III) is advantageous

24 in the perspective of long term storage.

25

1. Introduction

29 Acid Mine Drainage (AMD) is one of the worst environmental hazards resulting from

30 the extraction of base metals from sulfide deposits. These leachates result from the

31 oxidation of metal sulfides (especially pyrite) in mine tailings. The process releases

32 sulfate, iron and a range of toxic metals and metalloids, often including arsenic. This

33 element can be present at high concentrations in AMD, up to 350 mg L^{-1} (Paikaray,

34 2015; Williams, 2001). Arsenic contamination may be attenuated to some extent by

35 natural processes which involve biotic and abiotic Fe(II) oxidation and the subsequent

36 precipitation of Fe(III)-hydroxysulfates and Fe(III)-oxyhydroxides, together with

37 arsenite (As(III)) and arsenate (As(V)) adsorption and/or co-precipitation (Cheng et al.,

38 2009). The oxidation of arsenite into arsenate, which is efficiently mediated by bacteria

39 (Battaglia-Brunet et al., 2002; Bruneel et al., 2003) greatly improves As attenuation in

40 AMD. Indeed, the solubility of As(V)-Fe(III)-hydroxysulfates is lower than the

41 solubility of As(III)-Fe(III)-hydroxysulfates for a similar As/Fe ratio in the solid

42 (Maillot et al., 2013). These natural processes can serve as a basis for the passive

43 treatment of As-rich AMD if they are exploited in suitable systems. Passive treatments,

44 that do not require neither power nor constant maintenance, are particularly adapted to

2

45   remote locations. Numerous studies aimed to exploit microbial Fe(II) oxidation for the

46   removal of As from AMD in lab-scale bioreactors processing synthetic mine water (e.g.

47   Ahoranta et al., 2016; González-Contreras et al., 2012; Hedrich and Johnson, 2014).

48   Conversely, few trials have been attempted to exploit this process in field-pilot passive

49   bioreactors processing real AMD water (Elbaz-Poulichet et al., 2006; Macías et al.,

50   2012; Whitehead et al., 2005) (Table 1).

51   In the present study, we investigated arsenic removal from an AMD containing extreme

52   As concentrations (up to 140 mg L^{-1}) under the most mobile and toxic form, As(III)

53   (60–100 %, Casiot et al., 2003). The treatment consisted in a passive field-pilot

54   bioreactor exploiting iron oxidation by autochthonous bacterial communities, resulting

55   in the precipitation of Fe and As. The design of this reactor was derived from previous

56   laboratory experiments with a bench-scale channel bioreactor that provided up to 80 %

57   As removal during the treatment of AMD water originating from the same site

58   (Fernandez-Rojo et al., 2017). The two key parameters of the bioreactor design were 1)

59   a low water height above the precipitate and 2) a good oxygenation of the feed water

60   (Fernandez-Rojo et al., 2017). The field-pilot bioreactor was continuously fed during

61   six months with AMD by natural flow. The AMD was the spring of the Reigous Creek

62   at the Carnoulès mine in southern France (OREME, 2018), whose biogeochemistry and

63   microbial communities involved in Fe and As attenuation have been previously studied

64   (Bruneel et al., 2006,2011; Casiot et al., 2003; Egal et al., 2010; Volant et al., 2014).

65   We monitored inlet and outlet water physico-chemistry and the composition of Fe-As

66   precipitate, including arsenic redox state in water and precipitate. To estimate potential

67   microbial contribution to arsenite oxidation, the gene encoding the large subunit of the

68   As(III) oxidase (*aioA*) was quantified.

2. Materials and methods

2.1. Field-scale passive bioreactor

A flow pipe collected the AMD from its spring, located at the base of the Carnoulès tailings dam, and transferred it to the bioreactor, located 115 m down the way (mean slope of 5.9 %). At the bioreactor inlet, a small feed tank (52 cm length × 21 cm width × 26 cm height) limited the flow rate entering the bioreactor by means of a V-notch weir and a siphon. The level of water in the V-notch weir tank was constant and it was adjustable by the height of the siphon. The overflow was redirected to the Reigous Creek through a flow pipe (Figure 1A). The inlet flow rate decreased over short time intervals (~ one to two weeks) due to the inflow of sand particles into the AMD carrying pipes. Thus, cleaning these pipes was necessary after each sampling survey to restore the flow rate. Besides, a decantation tank was inserted upstream from the AMD intake after day 147 to limit the introduction of sand particles into the pipe.

Water circulation within the bioreactor was powered by natural flow. The bioreactor consisted of five shallow trays stacked head to tail on a shelf (Figure 1). Each tray sized 1.5 m^2 (1.5 × 1 m), 0.11 m depth, and it was made of 10 mm thick polyethylene sheets. Trays were divided into two compartments with a vertical separator leaving a 2 cm space at the bottom. The main compartment (1.2 × 1 m) was filled 3.5–4.5 cm in height with 80 kg of sand from river Moselle (uniformity coefficient 5.73, diameter at 10 % = 0.31 mm, at 60 % = 1.78 mm, at 85 % = 5.75 mm, $CaCO_3$ content = 0.19 %), in order to provide a support for microbial attachment. The overflow fell over from the outlet end of one tray to the inlet end of the next tray, through a polypropylene tube (2 cm i.d.),

4

91 thus favoring the water oxygenation. Water passed through the different trays (T1, T2,

92 T3, T4 and T5) before being discharged to the AMD stream.

2.2. Monitoring

94 The bioreactor was monitored during 194 days, between June 10th 2016 and December

95 21st 2016. Nine sampling surveys were made during the summer period (June, July),

96 one intermediate sampling in October, and four samplings during the autumn period

97 (November, December). At each sampling campaign, inlet and outlet waters were

98 collected. The following physico-chemical parameters were measured: pH, dissolved

99 oxygen concentration (DO), temperature, redox potential (Eh) and electrical

100 conductivity (EC). We also determined dissolved concentrations of Fe(II), total Fe,

101 As(III), As(V), and total As, after filtration (0.22 μm) and preservation using procedures

102 described in Fernandez-Rojo et al. (2017). We measured the flow rate and the water

103 height in each tray in order to estimate the apparent hydraulic retention time (HRT). The

104 apparent HRT was the mean of the maximum and the minimum HRT. To determine the

105 maximum HRT, we assumed that water flowed through the sand pores and that there

106 was no precipitate accumulation. On the contrary, for minimum HRT determination, we

107 considered that the sand pores were clogged and that there was a precipitate layer above

108 the sand.The maximum and the minimum HRT, expressed in hours, were calculated

109 with the following Equation (1):

$$Maximum/Minimum\ HRT = \frac{\sum_{i=1}^{n}(L_i * W_i) * (WH_i - PH_i) - \left(\frac{SW_i}{\delta} - \emptyset_i\right)}{Q} \qquad (1)$$

5

110 where "L_i" and "W_i" were the length and the width, respectively, in decimeters. "WH_i"

111 was the water height from the bottom of one tray measured in each sampling in

112 decimeters. "PH_i" was the precipitate height above the sand layer of one tray expressed

113 in decimeters. "SW_i" was the sand weight in kg, "δ" was the sand density in kg dm^{-3},

114 "$\emptyset$" was the sand vacuum volume in dm^3, and "Q" the water flow rate in dm^3 h^{-1}. "n"

115 corresponded to the number of trays (5) in the pilot. Details of these calculations are

116 given in the supporting information file.

117

2.3. Analyses

2.3.1. *Water samples*

120 All analytical procedures are detailed in Fernandez-Rojo et al. (2017). Briefly, the

121 concentrations of dissolved Fe(II) were determined using colorimetry at 510 nm after

122 complexation with 1,10-phenanthrolinium chloride. Total dissolved concentrations of

123 Fe, As and other elements (S (SO_4^{2-}), Al, Zn, and Pb) were determined using ICP-MS.

124 Arsenic redox speciation was determined using HPLC-ICP-MS.

125 The rates of Fe(II) oxidation, Fe- and As-removal (in mol L^{-1} s^{-1}) were calculated using

126 Equation (2):

$$\text{Rate} = \frac{([X]inlet - [X]outlet)}{HRT} \qquad (2)$$

127   where [X] was the concentration of dissolved Fe(II), total dissolved Fe, total dissolved

128   As, dissolved As(III) or dissolved As(V), respectively, in mol L^{-1} and HRT the apparent

129   hydraulic retention time in seconds.

130   Surface area is often a limitation in the design of passive treatments. To address this

131   issue and to compare with the literature data on water treatment processes (Table 1),

132   area-adjusted rates were calculated using Equation 3:

$$\text{Area} - \text{adjusted rate} = \frac{([X]inlet - [X]outlet) * Q}{Surface\ area} \qquad (3)$$

133   where the concentration of total dissolved Fe or total dissolved As ([X]) were expressed

134   in g L^{-1}, the flow rate (Q) in L d^{-1} and the surface area, in m^2. Only the 7.5 m^2 surface

135   above the sand layer was considered here because rapid clogging prevented water to

136   circulate through the sand layer.

2.3.2. *Solid samples*

138   When sampling the precipitate, the surface of each tray was divided in three zones

139   following the water flow path (Figure 1A): "A" refers to the 0.5 m^2 surface area close to

140   the inlet of each tray, "B" represents the 0.5 m^2 surface area in the middle section, and

141   "C" the 0.5 m^2 surface area close to the outlet of each tray. The precipitate from trays T1

142   to T5 was collected with a sterilized spatula by scraping the solid surface. The

143   precipitate was transferred into Falcon Tubes (50 mL) and centrifuged for 10 min at

144   4400 $\times$ *g* (Sorwall ST40, Thermo Scientific). The supernatant was discarded and the

145   precipitate was homogenized. A portion of the sample (~0.3 g) was dried in a vacuum

146   desiccator. Redox As determination was performed by HPLC-ICP-MS on a subsample

147 (100 mg) after extraction with orthophosphoric acid (Resongles et al., 2016). No fine

148 particles remained after this procedure, enabling total As and Fe determination. Another

149 subsample was used for X-ray diffraction (XRD) and a third one for quantification of

150 *aioA* gene copy numbers. These procedures were detailed in Fernandez-Rojo et al.

151 (2017).

2.4. Statistics

153 Friedman tests and Nemenyi post-hoc tests were performed with the XLSTAT 2018

154 software to compare the As/Fe molar ratio, the As(V)% and the number of *aioA*

155 genes/ng of DNA of the biogenic precipitate between the sampling dates.

156 Principal Component Analysis (PCA) was performed on functional parameters of the

157 pilot (As and Fe removal yields and rates) using the vegan package under R software

158 (version 3.4.0) and provided an ordination of data in factorial maps based on the scores

159 of the first two principal components. HRT and water physico-chemistry (inlet and

160 outlet temperature and DO, pH, Eh, conductivity, Fe and As concentration, Fe(II) to

161 total Fe proportion, As(III) to total As proportion) were fit to PCA ordinations in order

162 to identify the correlations between these variables and the functional parameters of the

163 pilot.

3. Results

3.1. Flow rate and hydraulic retention time

166 The HRT calculation relies mainly on the flow rate. This parameter exhibited important

167 variations, from 6 to 130 L h^{-1} in relation with partial clogging of the pipe carrying the

168 AMD to the bioreactor feed tank (Figure 2). The October survey (day 115) was

169 characterized by extremely low flow rate occurring after a two-month period without

170 flow pipe dredging. After day 147, a decantation tank was set up, resulting in a better

171 stabilization of the flow rate, between 30 and 49 L h^{-1}. The HRT calculation also relies

172 on the water height measured from the bottom of the trays. This parameter varied

173 between 34 and 112 mm. Indeed, the accumulation of precipitate within and over the

174 sand bed modified water discharge at the outlet of each tray, which subsequently

175 increased the water level within the tray. Consequently, the calculated apparent HRT

176 varied from 4 h to ~50 h (Figure 2).

3.2. Water physico-chemistry

177

3.2.1. *Inlet water*

178

179 Inlet water pH, DO and temperature exhibited notable variations over the monitoring

180 period (Figure 3). pH varied between 2.6 and 3.4 (Figure 3A). Dissolved oxygen

181 concentration was generally lower than 4 mg L^{-1} during the summer period (except on

182 day 45) and increased to 5.2 ± 0.3 mg L^{-1} in the autumn period (Figure 3B). The water

183 temperature was higher during the summer period (19 ± 3 °C) than during the autumn

184 period (11 ± 1 °C) (Figure 3C). Eh averaged 539 ± 30 mV (Figure 3D). Total dissolved

185 Fe and As concentrations increased respectively from 962 mg L^{-1} to 1314 mg L^{-1} and

186 from 111 to 152 mg L^{-1} during the summer period and then decreased to 801 ± 81 mg

187 L^{-1} (Fe) and 92 ± 10 mg L^{-1} (As) in the autumn period (Figure 3E-F). Both elements

188 were predominantly under the reduced redox state (more than 84 % Fe(II) and 78 %

189 As(III) (Figure S1B-D)). Dissolved sulfate and metal cations (Al, Zn, Pb)

190   concentrations in the inlet water averaged 2.8 ± 0.5 g L^{-1} (SO$_4^{2-}$), 47 ± 7 mg L^{-1} (Al), 21

191   ± 3 mg L^{-1} (Zn) and 1.5 ± 0.3 mg L^{-1} (Pb), respectively (Figure S1E-H).

192   ### 3.2.2. *Outlet water*

193   There was a decrease of pH up to 0.4 unit in the outlet water compared to the inlet

194   (Figure 3A). Water temperature between inlet and outlet varied within $\pm$ 4°C during

195   summer period, while a decrease (up to 7.3 °C) was always observed during the autumn

196   period (Figure 3C). Dissolved oxygen most systematically increased, by 5 mg L^{-1} at

197   most, between inlet and outlet (except on day 45). Fe removal yield did not exceed 11

198   % (Figure 3E) and up to 20 % Fe(II) was oxidized (Figure S1B)). Arsenic removal yield

199   ranged from 3 % to 97 % (Figure 3F). The corresponding removal rates varied from 5.7

200     $\times$ 10^{-9} to 1.6 $\times$ 10^{-7} mol L^{-1} s^{-1} for Fe (average rate $7 \pm 5 \times 10^{-8}$ mol L^{-1} s^{-1}) and from 1

201     $\times 10^{-8}$ to 3.2 $\times 10^{-8}$ mol L^{-1} s^{-1} for As (average rate $1.8 \pm 0.8 \times 10^{-8}$ mol L^{-1} s^{-1}) (Figure

202   4). Reduced Fe(II) and As(III) species remained predominant upon oxidized species in

203   the outlet water (more than 85% Fe(II) and 74% As(III)). The October data (day 115)

204   was an exception, with 98 % As(V) in the outlet water. Concentrations of dissolved Al,

205   Zn, S (SO$_4^{2-}$) and Pb also decreased between inlet and outlet, by less than 12 % for Al,

206   Zn, S and up to 45 % for Pb (Figure S1 E-H).

207   PCA illustrates the relationships between the functional parameters of the pilot (As and

208   Fe removal yields and rates) and the operating conditions including HRT and physico-

209   chemical variables (Figure 5). Days 115 to 194 (autumn period) were characterized by

210   the highest As removal yields, which were significantly correlated to HRT (p-

211   value < 0.001) and to inlet water DO concentration (p-value = 0.006). Days 11, 27 and

212 32 were characterized by the highest Fe removal yields, which were negatively

213 correlated (p-value = 0.025) to the proportion of Fe(II) to total Fe in inlet water.

3.3. Biogenic precipitate: mineralogy, molar As/Fe ratios, As redox state and *aioA* gene quantification

216 The precipitate recovered on the top of the sand layer contained quartz, mica, and

217 potassium feldspar all originating from the sand filter material (Figure 6). The Fe and

218 As content stabilized to 179 ± 39 mg Fe g^{-1} and 152 ± 33 mg As g^{-1} after 48 days (Table

219 S1). Tooeleite, a ferric arsenite sulfate mineral ($Fe_6(AsO_3)_4SO_4(OH)_4.4H_2O$) was the

220 only crystallized Fe-As phase identified. The XRD pattern also evidenced an

221 amorphous phase whose proportion increased at the expense of tooeleite, during the

222 monitoring period (Figure 6). The molar As/Fe ratio in the precipitate significantly

223 increased during the monitoring period from ~0.3 to ~0.7 in the three trays analyzed

224 (Figure 7A). The proportion of As(V) upon total As in the precipitate also increased

225 from ~20 % to ~85 % during the first 50 days, and then remained constant around

226 nearly 100 % until the end of the monitoring period (Figure 7B). The color of the

227 precipitate changed throughout time, from orange to pale yellow (Figure S2).

228 The relative abundance of arsenite oxidizing bacteria was assessed through the

229 quantification of *aioA* genes. A ten-fold increase of the number of *aioA* genes was

230 observed in the precipitate between day 11 and day 48. From this date, the number of

231 *aioA* genes remained relatively stable until the end of the monitoring period (Figure

232 7C).

4. Discussion

4.1. Arsenic and iron removal efficiency in the field-scale bioreactor

235   The field pilot removed 3 % to 97 % of total dissolved As from the Carnoulès AMD,

236   while Fe removal yield did not exceed 11 %. The HRT had a significant influence on As

237   removal yields; the important variations of HRT during the monitoring period are both

238   due to flow rate fluctuations and to water level variations inside the trays. The average

239   As removal rate ($(1.8 \pm 0.8) \times 10^{-8}$ mol L^{-1} s^{-1}) was close to our lab-scale experiments

240   rates (2×10^{-8} to 5×10^{-8} mol L^{-1} s^{-1}) (Fernandez-Rojo et al., 2017). For comparison, in

241   a laboratory bioreactor exploiting microbial Fe(II) oxidation, Ahoranta et al. (2016)

242   obtained an As removal rate of $\sim 1.5 \times 10^{-10}$ mol L^{-1} s^{-1} during the treatment of a

243   synthetic AMD containing 10 mg L^{-1} As(III) by adsorption onto biogenic jarosite at pH

244   3. Numerous factors, including water physico-chemistry, nature of precipitated solids,

245   and microbial communities might influence As removal rate in AMD (Asta et al., 2010,

246   2012). The Fe removal rate ($(7 \pm 5) \times 10^{-8}$ mol L^{-1} s^{-1}) in the field pilot was within the

247   lower range of lab-scale experiments rates (1.8 to 24×10^{-8} mol L^{-1} s^{-1}, Fernandez-Rojo

248   et al. (2017)). The field pilot oxidized less than 20 % Fe(II) whatever the HRT (Figure

249   S1-B), compared to nearly 100 % in the lab-scale pilot (Fernandez-Rojo et al., 2017).

250   There was no link between Fe removal yield and HRT or inlet water DO (Figure 5).

251   Thus, the system appeared not very effective regarding Fe oxidation and removal. One

252   possible explanation is the large water height (15−70 mm) above the precipitate. We

253   demonstrated in our lab-scale bioreactor that large water height limits oxygen

254   availability (and then Fe(II) oxidation and subsequent Fe precipitation) at the

12

255 water/precipitate interface, due to faster metabolic consumption, relative to the oxygen

256 diffusion (Fernandez-Rojo et al., 2017).

257 A few *in situ* devices exploiting microbial or abiotic Fe(II) oxidation have been

258 experienced so far for arsenic removal in AMD in a passive way (Table 1). They were

259 in the form of ponds (Elbaz-Poulichet et al., 2006), lagoons (Macías et al., 2012) or

260 wetlands (Hamilton et al., 1999; Whitehead et al., 2005). Some of them were preceded

261 by closed or open channels or drains filled with alkaline rocks (Caraballo et al., 2009;

262 Gusek et al., 1994; Rötting et al., 2008) in order to promote rapid abiotic Fe(II)

263 oxidation at near-neutral pH prior to As retention (Table 1). Most of these systems

264 achieved more than 80 % removal for AMD containing low As concentrations (< 3

265 mg L^{-1}). Area-adjusted arsenic removal rates obtained in the present study were higher

266 (3–12 g m^{-2} d^{-1}) than those described in previous studies, in relation with higher

267 dissolved arsenic content. The high As concentration of the Carnoulès AMD is

268 particularly challenging. In a previous field-pilot experiment in Carnoulès, only 13–20

269 % As removal was achieved (Elbaz-Poulichet et al., 2006). The present bioreactor

270 showed a substantial improvement of As removal yield.

4.2. As-bearing phases formed in the pilot

272 Tooeleite and an amorphous-Fe-As phase were identified in the biogenic precipitate of

273 the field-pilot. These mineral phases have been observed for years in the upstream

274 section of Reigous Creek, in fresh and dry sediments, and in laminated concretions

275 (Morin et al., 2003; Egal et al., 2010). These solid phases were favored upon the most

276 widespread As-schwertmannite due to the As/Fe ratio exceeding 0.3 in the precipitate.

277 Indeed, an As/Fe ratio higher than 0.15 was shown to disrupt the crystallization of

13

278 As(V)-schwertmannite (Carlson et al., 2002). In the field-pilot, tooeleite was replaced

279 over time by an amorphous phase subsequently to As(V) enrichment in the precipitate

280 (Figure 6; Table S1), consistently with the study of Liu et al. (2015). These authors

281 found that the crystallinity of tooeleite decreased with increasing As(V)/As(III) ratio

282 and no more tooeleite was detected on the XRD spectrum when the As(V)/As(III) ratio

283 exceeded 0.4 (Liu et al., 2015). The latter conditions occurred after day 19 in the present

284 experiment, with As(V)/As(III) ratio in the precipitate increasing beyond 0.7. This is

285 consistent with the formation of an amorphous ferric arsenate phase. Future work

286 should examine whether the characteristics of As-bearing phases (As content, As/Fe

287 ratio and mineralogy) and their evolution over the long-term constitute limiting factors

288 in the achievement of the lowest As concentration in the treated water.

289 **4.3. Arsenic oxidation**

290 As(III) was predominant (> 78 %) over As(V) in the feed water and both As(III) and

291 As(V) species were removed from the dissolved phase in similar proportion in the

292 bioreactor (Figure S1C-D). Conversely, As(V) was predominant (> 50 %) over As(III)

293 in the precipitate after 20 days functioning and reached nearly one hundred percent in

294 trays T1-C, T2-C and T5-C after 170 days (Figure 7B; Table S1). Thus, As(III)

295 appeared to be oxidized within the field pilot. Both biotic and abiotic As(III) oxidation

296 may be involved. Abiotic As(III) oxidation may occur in presence of dissolved Fe(III)

297 (Asta et al., 2012; Emett and Khoe, 2001) or at the surface of Fe(III) minerals (Bhandari

298 et al., 2011; 2012; Paikaray et al., 2014; Pozdnyakov et al., 2016; Sun and Doner, 1998)

299 in acidic environments in presence of light. However, batch experiments conducted with

300 AMD waters from Carnoulès showed that the photochemical oxidation was negligible

14

301 compared to the biological oxidation (Egal et al., 2009). Similar results were obtained

302 by other authors in an acid hydrothermal discharge (Leiva et al., 2014).

303 Furthermore, the temporal increase of the As-oxidation genetic potential (expressed as

304 the number of copies of *aioA* genes/ng of DNA) during the first 50 days (Figure 6C)

305 strongly suggests the establishment of As(III)-oxidizing bacteria in the biogenic

306 precipitate. The As(III)-oxidizing *Thiomonas* spp. have proved to be active members of

307 the bacterial community in the Reigous Creek (Bruneel et al., 2011). They are the only

308 arsenite oxidizers described so far in Carnoulès where they express *in situ* their arsenite

309 oxidation activity catalyzed by the AioA enzyme (Hovasse et al., 2016). We can

310 therefore hypothesize that arsenite oxidation occurring in the bioreactor is mainly

311 biological.

5. Conclusion and perspectives

313 The present field system provided As removal at a similar rate than the lab-scale pilot.

314 However, the water circulation in the system must be improved to stabilize the HRT in

315 future work. Fe oxidation and precipitation yield appeared to be limited by the large

316 water height above the precipitate. Nevertheless, the low amount of iron precipitated

317 (maximum 11 %), compared to other systems where the AMD is neutralized, enables

318 the production of low amounts of sludge, highly concentrated in arsenic (up to 20 % dry

319 weight), thus limiting the cost of As-rich sludge disposal in engineered hazardous

320 wastes landfill facilities. The nature of the As-bearing phases produced, mainly

321 amorphous ferric arsenate, is advantageous in the perspective of long-term storage of

322 these treatment sludges. This solid phase has a high As load and a low solubility

323 compared to As(III)-Fe(III) phases (Langmuir et al., 2006; Virčíková et al., 1995;

15

324 Maillot et al., 2013). However, the influence of storage conditions on sludge stability

325 needs to be fully evaluated.

326 Future efforts should focus on As removal rate improvement. For this, higher

327 oxygenation should be tested, together with the introduction in the trays of a physical

328 support with high pore volume, such as pozzolana, to prevent fast clogging and to

329 maximize surface area of Fe-and As-oxidizing biofilm per unit of water volume

330 (Battaglia-Brunet et al., 2006). In the perspective of upscaling of the treatment unit,

331 long-term monitoring would be necessary to explore possible seasonal variation of the

332 removal yields and As redox state in the precipitate. Long-term monitoring would also

333 provide information on the frequency of sludge removal from the system. Furthermore,

334 the spatio-temporal dynamic of bacteria involved in Fe(II) and As(III) oxidation such as

335 *Thiomonas* spp. in the present field-scale pilot deserves further research.

336 This treatment could be implemented as one step targeting arsenic in a multi-step AMD

337 treatment. Indeed, iron, sulfate and metal cations (Al, Zn, Pb) are only partially removed

338 by this treatment and outlet pH remains acid (pH~3). A sulfate reduction bioreactor

339 could be implemented to raise the pH and selectively recover zinc in the form of sulfide

340 (Chen et al., 2016; Hedrich and Johnson, 2014; Le Pape et al., 2017). A finish treatment

341 such as Dispersed alkaline substrate (DAS) and decantation ponds might be used to

342 further raise the pH and remove remaining Fe, Al, and other metal cations, before

343 discharge into natural water bodies (Caraballo et al., 2011, 2009; Rötting et al., 2008).

344 **Acknowledgements**

16

355

References

Ahoranta, S.H., Kokko, M.E., Papirio, S., Özkaya, B., Puhakka, J.A., 2016. Arsenic removal from acidic solutions with biogenic ferric precipitates. J. Hazard. Mater. 306, 124–132. doi:10.1016/j.jhazmat.2015.12.012

Asta, M.P., Ayora, C., Acero, P., Cama, J., 2010. Field rates for natural attenuation of arsenic in Tinto Santa Rosa acid mine drainage (SW Spain). J. Hazard. Mater. 177, 1102–1111. doi:10.1016/j.jhazmat.2010.01.034

Asta, M.P., Kirk Nordstrom, D., Blaine McCleskey, R., 2012. Simultaneous oxidation of arsenic and antimony at low and circumneutral pH, with and without microbial catalysis. Appl. Geochem. 27, 281–291. doi:http://dx.doi.org/10.1016/j.apgeochem.2011.09.002

Battaglia-Brunet, F., Dictor, M.-C., Garrido, F., Crouzet, C., Morin, D., Dekeyser, K., Clarens, M., Baranger, P., 2002. An arsenic(III)-oxidizing bacterial population: selection, characterization, and performance in reactors. J. Appl. Microbiol. 93, 656–667. doi:10.1046/j.1365-2672.2002.01726.x

Battaglia-Brunet, F., Itard, Y., Garrido, F., Delorme, F., Crouzet, C., Greffie, C., Joulian, C., 2006. A simple biogeochemical process removing arsenic from a mine drainage water. Geomicrobiol. J. 23, 201–211. doi:10.1080/01490450600724282

Bhandari, N., Reeder, R.J., Strongin, D.R., 2011. Photoinduced oxidation of arsenite to arsenate on ferrihydrite. Environ. Sci. Technol. 45, 2783–2789. doi:10.1021/es103793y

Bhandari, N., Reeder, R.J., Strongin, D.R., 2012. Photoinduced oxidation of arsenite to arsenate on goehite. Environ. Sci. Technol. 46, 8044–8051. doi:/10.1021/es300988p

Bruneel, O., Personné, J.C., Casiot, C., Leblanc, M., Elbaz-Poulichet, F., Mahler, B.J., Le Flèche, A., Grimont, P.A.D., 2003. Mediation of arsenic oxidation by *Thiomonas* sp. in acid-mine drainage (Carnoulès, France). J. Appl. Microbiol. 95, 492–499. doi :10.1046/j.1365-2672.2003.02004.x

Bruneel, O., Duran, R., Casiot, C., Elbaz-Poulichet, F., Personné, J.C., 2006. Diversity of microorganisms in Fe-As-rich acid mine drainage waters of Carnoulès, France. Appl. Environ. Microbiol. 72, 551–556. doi:10.1128/AEM.72.1.551-556.2006

Bruneel, O., Volant, A., Gallien, S., Chaumande, B., Casiot, C., Carapito, C., Bardil, A., Morin, G., Brown Jr., G.E., Personné, J.C., Le Paslier, D., Schaeffer, C., Van Dorsselaer, A., Bertin, P.N., Elbaz-Poulichet, F., Arsène-Ploetze, F., 2011. Characterization of the active bacterial community involved in natural attenuation processes in arsenic-rich creek sediments. Microb. Ecol. 61, 793–810. doi:10.1007/s00248-011-9808-9

18

Caraballo, M.A., Rötting, T.S., Macías, F., Nieto, J.M., Ayora, C., 2009. Field multi-step limestone and MgO passive system to treat acid mine drainage with high metal concentrations. Appl. Geochem. 24, 2301–2311. doi:10.1016/j.apgeochem.2009.09.007

Caraballo, M.A., Macías, F., Rötting, T.S., Nieto, J.M., Ayora, C., 2011. Long term remediation of highly polluted acid mine drainage: A sustainable approach to restore the environmental quality of the Odiel river basin. Environ. Pollut. 159, 3613–3619. doi:10.1016/j.envpol.2011.08.003

Carlson, L., Bigham, J.M., Schwertmann, U., Kyek, A., Wagner, F., 2002. Scavenging of As from acid mine drainage by schwertmannite and ferrihydrite: a comparison with synthetic analogues. Environ. Sci. Technol. 36, 1712–1719.doi:10.1021/es0110271

Casiot, C., Morin, G., Juillot, F., Bruneel, O., Personné, J.-C., Leblanc, M., Duquesne, K., Bonnefoy, V., Elbaz-Poulichet, F., 2003. Bacterial immobilization and oxidation of arsenic in acid mine drainage (Carnoulès creek, France). Water Res. 37, 2929–2936. doi:http://dx.doi.org/10.1016/S0043-1354(03)00080-0

Chen, C.-J., Jiang, W.-T., 2012. Influence of waterfall aeration and seasonal temperature variation on the iron and arsenic attenuation rates in an acid mine drainage system. Appl. Geochem. 27, 1966–1978. doi:http://dx.doi.org/10.1016/j.apgeochem.2012.06.003

Chen, L.-X., Huang, L.-N., Méndez-García, C., Kuang, J.-L., Hua, Z.-S., Liu, J., Shu, W.-S., 2016. Microbial communities, processes and functions in acid mine drainage ecosystems. Curr. Opin. Biotechnol. 38, 150–158. doi:10.1016/j.copbio.2016.01.013

Cheng, H., Hu, Y., Luo, J., Xu, B., Zhao, J., 2009. Geochemical processes controlling fate and transport of arsenic in acid mine drainage (AMD) and natural systems. J Hazard Mater. 165, 13-26. doi: 10.1016/j.jhazmat.2008.10.070.

Egal, M., Casiot, C., Morin, G., Parmentier, M., Bruneel, O., Lebrun, S., Elbaz-Poulichet, F., 2009. Kinetic control on the formation of tooeleite, schwertmannite and jarosite by *Acidithiobacillus ferrooxidans* strains in an As(III)-rich acid mine water. Chem. Geol. 265, 432–441. doi:10.1016/j.chemgeo.2009.05.008

Egal, M., Casiot, C., Morin, G., Elbaz-Poulichet, F., Cordier, M.-A., Bruneel, O., 2010. An updated insight into the natural attenuation of As concentrations in Reigous Creek (southern France). Appl. Geochem. 25, 1949–1957. doi:http://dx.doi.org/10.1016/j.apgeochem.2010.10.012

Elbaz-Poulichet, F., Bruneel, O., Casiot, C., 2006. The Carnoulès mine. Generation of As-rich acid mine drainage, natural attenuation processes and solutions for passive in-situ remediation, in: Difpolmine (Diffuse Pollution From Mining Activities).

Emett, M.T., Khoe, G.H., 2001. Photochemical oxidation of arsenic by oxygen and iron in acidic solutions. Water Res. 35, 649–656. doi:http://dx.doi.org/10.1016/S0043-

433   1354(00)00294-3

434   Fernandez-Rojo, L., Héry, M., Le Pape, P., Braungardt, C., Desoeuvre, A., Torres, E.,
435   Tardy, V., Resongles, E., Laroche, E., Delpoux, S., Joulian, C., Battaglia-Brunet,
436   F., Boisson, J., Grapin, G., Morin, G., Casiot, C., 2017. Biological attenuation of
437   arsenic and iron in a continuous flow bioreactor treating acid mine drainage
438   (AMD). Water Res. 123, 594–606. doi:10.1016/j.watres.2017.06.059

439   González-Contreras, P., Weijma, J., Buisman, C.J.N., 2012. Continuous bioscorodite
440   crystallization in CSTRs for arsenic removal and disposal. Water Res. 46, 5883–
441   5892. doi:10.1016/j.watres.2012.07.055

442   Gusek, J.J., Gormley, J.T., Scheetz, J.W., 1994. Design and construction aspects of
443   pilot-scale passive treatment systems for acid rock drainage at metal mines.
444   Hydrometallurgy 777–793. doi:10.1007/978-94-011-1214-7

445   Hamilton, Q.U.I., Lamb, H.M., Hallett, C., Proctor, J. a., 1999. Passive treatment
446   systems for the remediation of acid mine drainage at Wheal Jane, Cornwall. Water
447   Environ. J. 13, 93–103. doi:10.1111/j.1747-6593.1999.tb01014.x

448   Hedrich, S., Johnson, D.B., 2014. Remediation and selective recovery of metals from
449   acidic mine waters using novel modular bioreactors. Environ. Sci. Technol. 48,
450   12206–12212. doi:10.1021/es5030367

451   Hovasse, A., Bruneel, O., Casiot, C., Desoeuvre, A., Farasin, J., Hery, M., Van
452   Dorsselaer, A., Carapito, C., Arsène-Ploetze, F., 2016. Spatio-temporal detection
453   of the *Thiomonas* population and the *Thiomonas arsenite oxidase* involved in
454   natural arsenite attenuation processes in the Carnoulès acid mine drainage. Front.
455   Cell Dev. Biol. 4, 1–14. doi:10.3389/fcell.2016.00003

456   Langmuir, D., Mahoney, J., Rowson, J., 2006. Solubility products of amorphous ferric
457   arsenate and crystalline scorodite ($FeAsO_4 \cdot 2H_2O$) and their application to arsenic
458   behavior in buried mine tailings. Geochim. Cosmochim. Acta 70, 2942–2956.
459   doi:10.1016/j.gca.2006.03.006

460   Leiva, E.D., Rámila, C. d P., Vargas, I.T., Escauriaza, C.R., Bonilla, C.A., Pizarro,
461   G.E., Regan, J.M., Pasten, P.A., 2014. Natural attenuation process via microbial
462   oxidation of arsenic in a high Andean watershed. Sci. Total Environ. 466–467,
463   490–502. doi:10.1016/j.scitotenv.2013.07.009

464   Le Pape, P., Battaglia-Brunet, F., Parmentier, M., Joulian, C., Gassaud, C., Fernandez-
465   Rojo, L., Guigner, J.-M., Ikogou, M., Stetten, L., Olivi, L., Casiot, C., Morin, G.,
466   2017. Complete removal of arsenic and zinc from a heavily contaminated acid
467   mine drainage via an indigenous SRB consortium. J. Hazard. Mater. 321, 764–772.
468   doi:10.1016/j.jhazmat.2016.09.060

469   Liu, J., Deng, S., Zhao, F., Cheng, H., Frost, R.L., 2015. Spectroscopic characterization
470   and solubility investigation on the effects of As(V) on mineral structure tooeleite
471   ($Fe_6(AsO_3)_4SO_4(OH)_4 \cdot H_2O$). Spectrochim. Acta A Mol. Biomol. Spectrosc. 134,
472   428–433. doi:10.1016/j.saa.2014.06.111

473 Macías, F., Caraballo, M.A., Nieto, J.M., Rötting, T.S., Ayora, C., 2012. Natural
474   pretreatment and passive remediation of highly polluted acid mine drainage. J.
475   Environ. Manage. 104, 93–100.
476   doi:http://dx.doi.org/10.1016/j.jenvman.2012.03.027

477 Maillot, F., Morin, G., Juillot, F., Bruneel, O., Casiot, C., Ona-Nguema, G., Wang, Y.,
478   Lebrun, S., Aubry, E., Vlaic, G., Brown Jr., G.E., 2013. Structure and reactivity of
479   As(III)- and As(V)-rich schwertmannites and amorphous ferric arsenate sulfate
480   from the Carnoulès acid mine drainage, France: comparison with biotic and abiotic
481   model compounds and implications for As remediation. Geochim. Cosmochim.
482   Acta 104, 310–329. doi:10.1016/j.gca.2012.11.016.

483 Morin, G., Juillot, F., Casiot, C., Bruneel, O., Personné, J.-C., Elbaz-Poulichet, F.,
484   Leblanc, M., Ildefonse, P., Calas, G., 2003. Bacterial formation of tooeleite and
485   mixed arsenic(III) or arsenic(V)−iron(III) gels in the Carnoulès acid mine drainage,
486   France. A XANES, XRD, and SEM study. Environ. Sci. Technol. 37, 1705–1712.
487   doi:10.1021/es025688p

488 OREME, observatoire de l'ancien site minier de Carnoulès (2018).
489   https://data.oreme.org/carnoules/home (accessed on November 19th 2018).

490 Paikaray, S., Essilfie-Dughan, J., Göttlicher, J., Pollok, K., Peiffer, S., 2014. Redox
491   stability of As(III) on schwertmannite surfaces. J. Hazard. Mater. 265, 208–216.
492   doi:10.1016/j.jhazmat.2013.11.068

493 Paikaray, S., 2015. Arsenic geochemistry of acid mine drainage. Mine Water Environ.
494   34, 181−196. doi:10.1007/s10230-014-0286-4

495 Pozdnyakov, I.P., Ding, W., Xu, J., Chen, L., Wu, F., Grivin, V.P., Plyusnin, V.F.,
496   2016. Photochemical transformation of an iron(III)-arsenite complex in acidic
497   aqueous solution. Photochem. Photobiol. Sci. 15, 431–439.
498   doi:10.1039/c5pp00240k

499 Resongles, E., Le Pape, P., Fernandez-Rojo, L., Morin, G., Brest, J., Guo, S., Casiot, C.,
500   2016. Routine determination of inorganic arsenic speciation in precipitates from
501   acid mine drainage using orthophosphoric acid extraction followed by HPLC-ICP-
502   MS. Anal. Methods 8, 7420–7426. doi:10.1039/c6ay02084d

503 Rötting, T.S., Caraballo, M.A., Serrano, J.A., Ayora, C., Carrera, J., 2008. Field
504   application of calcite Dispersed Alkaline Substrate (calcite-DAS) for passive
505   treatment of acid mine drainage with high Al and metal concentrations. Appl.
506   Geochem. 23, 1660–1674. doi:10.1016/j.apgeochem.2008.02.023

507 Sun, X., Doner, H.E., 1998. Adsorption and oxidation of arsenite on goethite. Soil Sci.
508   163, 278−287. doi:10.1097/00010694-199804000-00003

509 Virčíková, E., Molnár, Ľ., Lech, P., Reitznerová, E., 1995. Solubilities of amorphous
510   Fe-As precipitates. Hydrometallurgy 38, 111–123.
511   doi:http://dx.doi.org/10.1016/0304-386X(94)00072-B

512 Volant, A., Bruneel, O., Desoeuvre, A., Héry, M., Casiot, C., Bru, N., Delpoux, S.,
513   Fahy, A., Javerliat, F., Bouchez, O., Duran, R., Bertin, P.N., Elbaz-Poulichet, F.,
514   Lauga, B., 2014. Diversity and spatiotemporal dynamics of bacterial communities:
515   physicochemical and other drivers along an acid mine drainage. FEMS Microbiol.
516   Ecol. 90, 247–263. doi:10.1111/1574-6941.12394

517 Whitehead, P.G., Hall, G., Neal, C., Prior, H., 2005. Chemical behaviour of the Wheal
518   Jane bioremediation system. Sci. Total Environ. 338, 41–51.
519   doi:10.1016/j.scitotenv.2004.09.004

520 Williams, M., 2001. Arsenic in mine waters: an international study. Environ. Geol. 40,
521   267–278. doi:10.1007/s002540000162

1
2
3
4
5
6
7
8
9
10
11
12
13
14
15
16
17
18
19
20
21
22
23
24
25
26
27
28
29
30
31
32
33
34
35
36
37
38
39
40
41
42
43
44
45
46
47
48
49
50
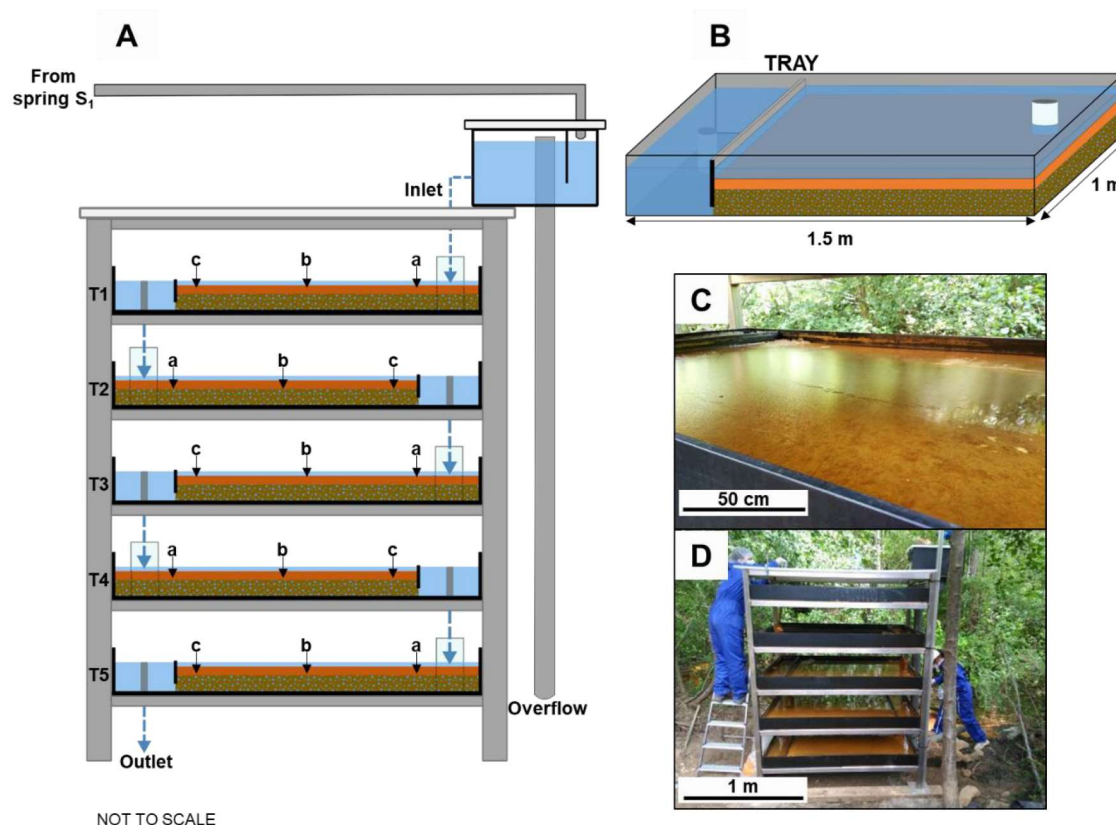51
52
53
54
55
56
57
58
59
60
61
62
63
64
65

22

Figure 1. Schematic representation of the field bioreactor with the five trays (T = tray) (A) and detail of each tray (B). Pictures of one of the trays showing the orange biogenic precipitate below the thin water layer (C), and of the whole field bioreactor (D) from June 2016. Letters a, b and c in (A) indicate the biogenic precipitates sampling locations.
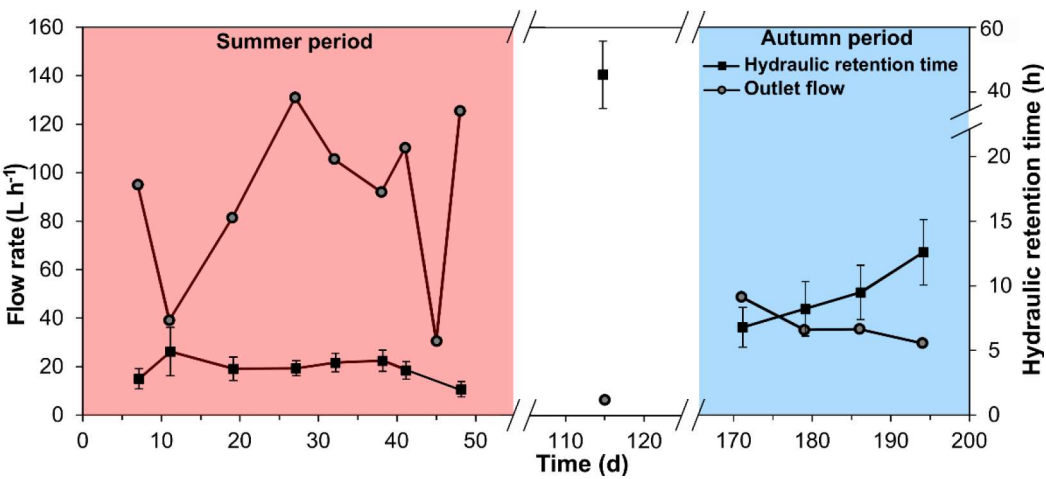
Figure 2
Click here to download Figure: 20181014_Figure 2.docx

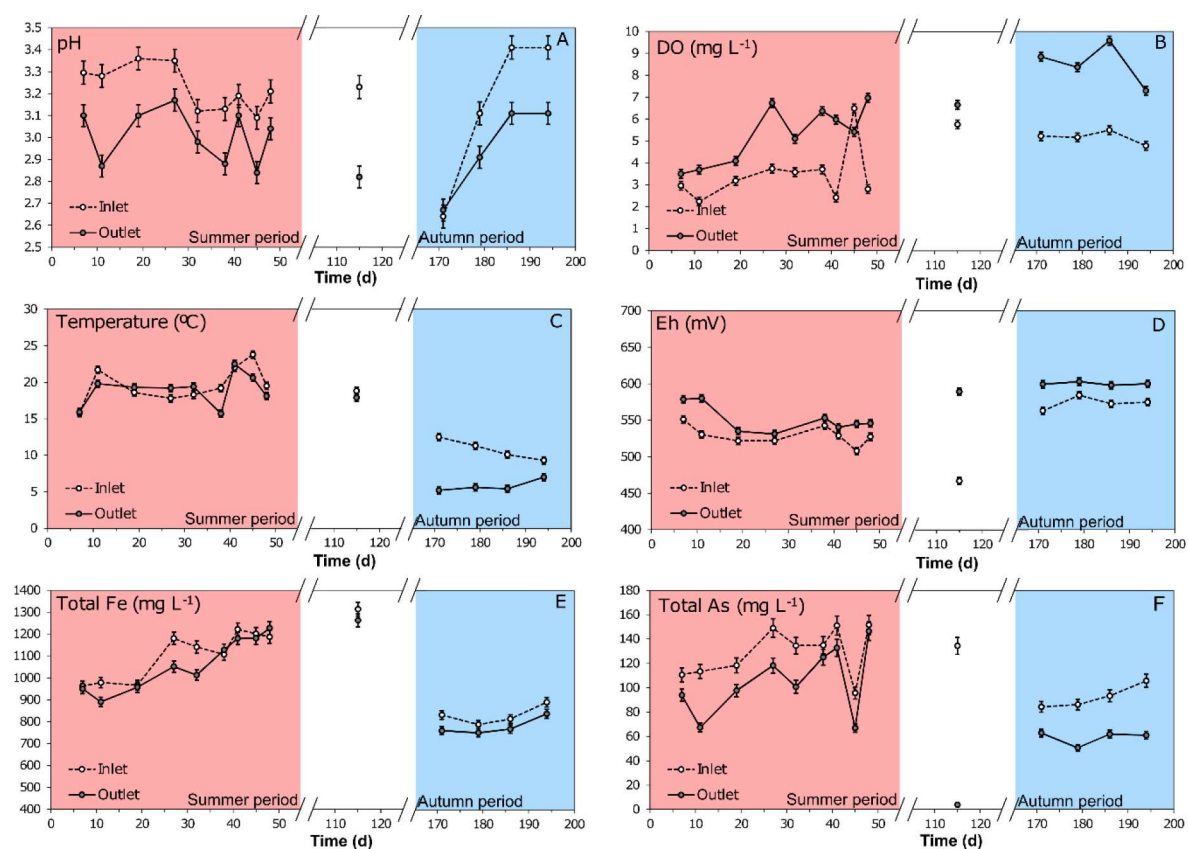Figure 2. Variation of the flow rate during the monitoring period and estimation of the HRT.

Figure 3. Monitoring of inlet and outlet water pH (A), dissolved oxygen concentration (B), temperature (C), redox potential (D), total dissolved Fe concentration (E), and total dissolved As concentration (F) in the field bioreactor.
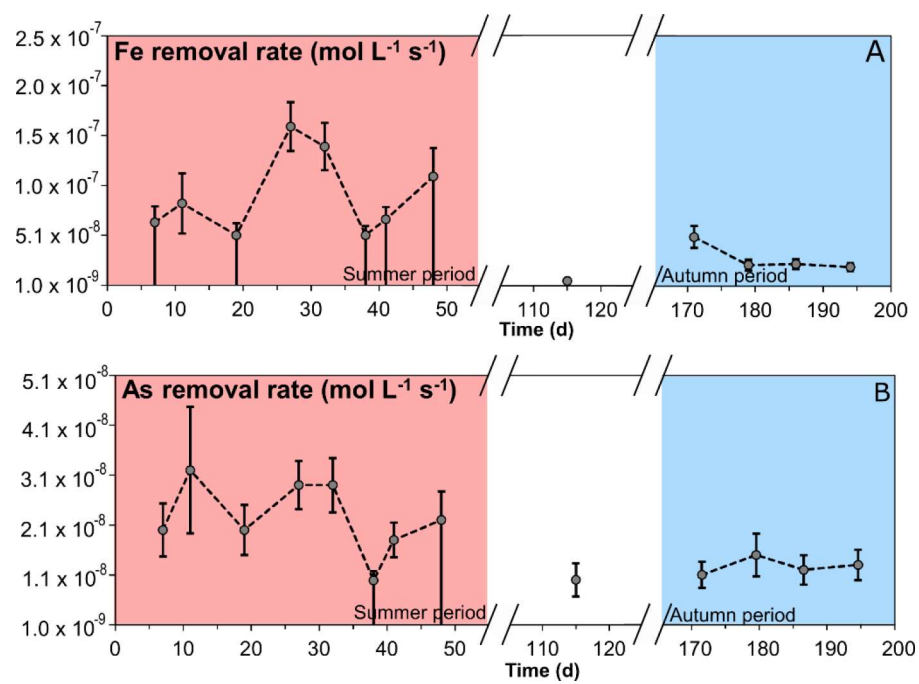
Figure 4. Monitoring of the Fe (A) and As removal rates (B) in the field bioreactor. Rate values represented by a high negative SD correspond to maximum removal rates estimated from the analytical detection limit (no significant total Fe or total As concentration decrease between inlet and outlet).
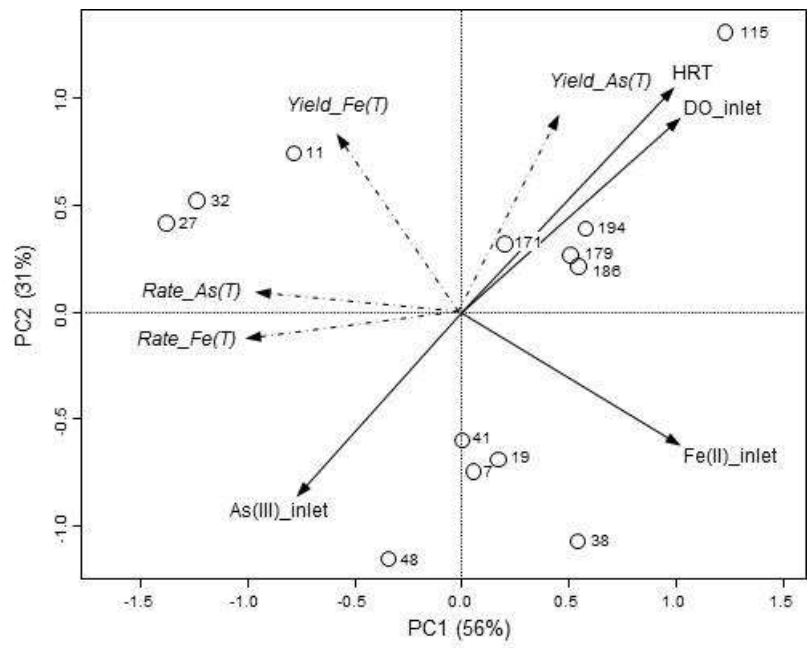
Figure 5. Principal Component Analysis (PC1 × PC2) based on functional parameters (total As and total Fe removal yields and rates) of the bioreactor across time. Circles with numbers represent the sampling days after the bioreactor setup. Vectors in the bi-plot overlay were constructed from a data frame containing HRT and water physico-chemistry parameters (inlet and outlet temperature, DO, pH, Eh, conductivity, Fe and As concentrations and proportions of Fe(II) to total Fe and As(III) to total As). Only correlations with p-values ≤ 0.05 were included. The angle and length of the vector indicate the direction and strength of the variable.
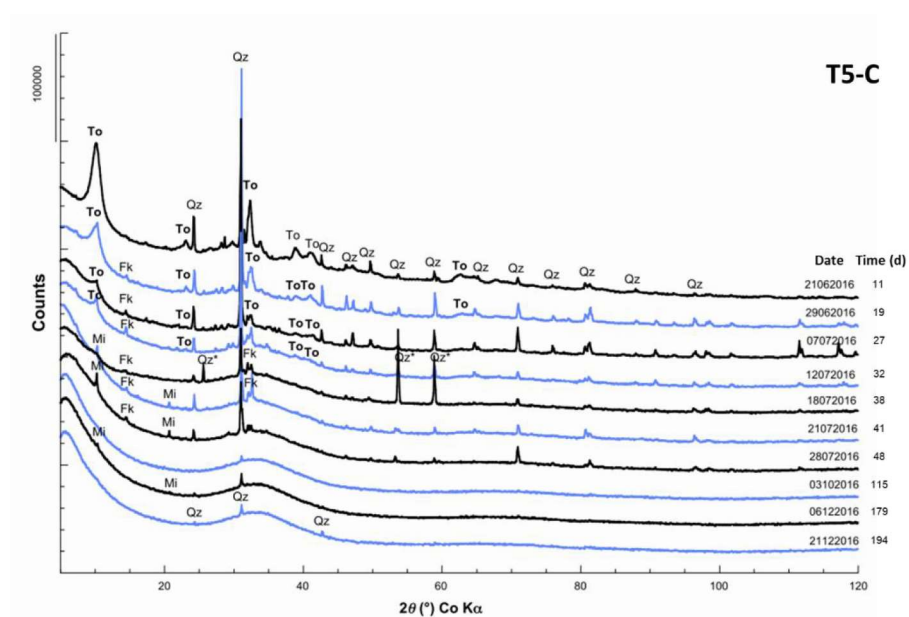
Figure 6. Evolution of X-ray diffractograms on the biogenic precipitate in tray T5-C during the monitoring period. Qz = quartz, To = tooeleite, Fk = potassium feldspar, Mi = micas.

Figure 7
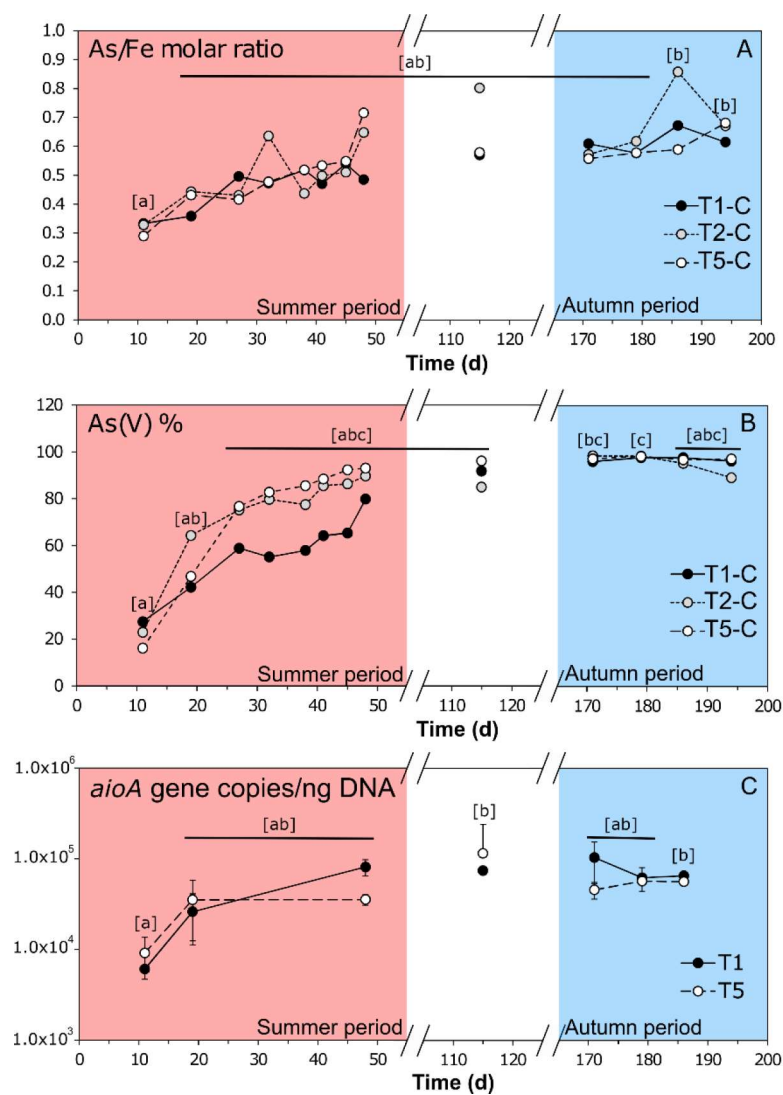Click here to download Figure: 20181014_Figure 7.docx

Figure 7. Evolution of As/Fe molar ratio (A) and As(V) percentage (B) in the biogenic precipitate from trays T1-C, T2-C, and T5-C during the monitoring period. Evolution of number of *aioA* gene copies/ng of DNA for trays T1 and T5 (A, B, and C section samples) during the same time (C). Different letters in brackets indicate statistically significant differences according to Friedman (p-value < 0.05) and Nemenyi multiple pairwise comparisons tests.

Table 1. Comparison with other field trials exploiting biological or chemical Fe precipitation and As removal from AMD water in passive treatment devices

Reference	Site	Whole design	System evaluated	Influent pH	Influent As (mg L⁻¹)	Influent Fe (mg L⁻¹)	As removal %	Fe removal %	As removal rate (g m⁻² d⁻¹)	Fe removal rate (g m⁻² d⁻¹)	HRT (h)	Mineralogy	As/Fe molar ratio or As concentration in the solid phase
Biological treatments													
This study	Carnoulès mine (France)	5 aerobic ponds stacked on top of each other connected by cascades	Whole system	2.6–3.5	85–150	790–1320	3–97	<0–11	2–13	<0–54	2.3–50	Tooeleite, Amorphous ferric arsenate	0.29–0.86
Elbaz-Poulichet et al. (2006)	Carnoulès mine (France)	Aerobic pond (3 different configurations a) with ridges, b) shallow pond, c) with cascades) + decantation pond (DP) + anaerobic wetland	Aerobic ponds	2.5–4.5	50–250	800–1200	11–20	n.s.	5–10	n.s.	0.5–3	n.s.	n.s.
Macías et al. (2012)	Monte Romero mine (Spain)	Natural iron oxidizing lagoon (NFOL) + dispersed alkaline substrate (DAS) + 2 DP joined by cascades + DAS	NFOL	~3	0.1–1	275 (99 % Fe(II))	80	38	0.1–1*	100*	n.s.	Sch, goe (from Phreeqc calculations)	0.002*
Hamilton et al. (1999)	Wheal Jane mine (UK)	5 aerobic wetlands + anaerobic pond + rock filter	5 aerobic wetlands	~4	2.4	~140	> 99	74	n.s.	1.2	n.s.	n.s.	n.s.
Whitehead et al. (2005)	Wheal Jane mine (UK)	5 aerobic wetlands + anaerobic pond + rock filter	5 aerobic wetlands	3.8	2.7	144	> 99*	75*	n.s.	5.8 (first unit)	n.s.	n.s.	< 0.1 % As (first aerobic cell)
Kalin and Caetano Chaves (2003)	Nova Lima mining district (Brazil)	4 oxidation-precipitation-settling ponds + 3 anaerobic ponds	first oxidation-precipitation-settling pond	2–4	< LD	20–300	n.s.	15–38 (4 aerobic ponds)	~0.004	~11	48	n.s.	~0.0004* (4 aerobic ponds)
Chemical treatments													
Rötting et al. (2008)	Monte Romero mine (Spain)	DAS+ 3 DP joined by cascades	DAS	3.0-3.9	0.1-1.5	290–357 (95 % Fe(II))	99	48 (whole system)	0.05–0.75*	n.s.	24	Sch, goe (0–3 cm depth)	~0.002* (0–3 cm depth)
Caraballo et al. (2009)	Monte Romero mine (Spain)	DAS + 2 DP joined by cascades + DAS + 2 DP joined by cascades + DAS (MgO)	1ˢᵗ DAS	3.08	0.3	358	> 99	34 (1* DAS+ 2 DP)	n.s.	n.s.	24 h	Sch, goe (0–3 cm depth)	n.s.
Gusek et al. (1994)	Leviathan mine (USA)	ALD, 3 aerobic pond, anaerobic pond	Whole system	4.5	0.1	340	90	99	n.s.	n.s.	n.s.	n.s.	n.s.

*Calculated
n.s. = not specified
LD = limit of detection
Sch = schwertmannite, Goe = goethite